water

MDPI

Article

Multi-Level Data Analyses for Characterizing Rainfall-Induced Landslide Scenarios: The Example of Catanzaro Municipality (South Italy)

Olga Petrucci [1], Graziella Emanuela Scarcella [2] and Massimo Conforti [1,*]

[1] CNR-IRPI Research Institute for Geo-Hydrological Protection, Via Cavour 4–6, 87036 Rende, Italy; olga.petrucci@irpi.cnr.it
[2] Department of Informatics, Modelling, Electronics and System Engineering, University of Calabria, Via P. Bucci, cubo 42/C, 87036 Rende, Italy; graziellascarcella90@gmail.com
* Correspondence: massimo.conforti@irpi.cnr.it

Abstract: This paper presents a GIS-based approach to create a multilevel data system for detailed knowledge of landslide occurrences in small territorial units such as municipalities. The main aim is to collect all the available data (geological, geomorphological, and climatic data, as well as landslide inventory maps and catalogues) in a structured data management system and perform further analyses to identify the typical landslide scenarios of the study area that can be useful in landslide risk management. We demonstrated the use of the methodology analyzing landslide risk in the municipality of Catanzaro (southern Italy), having a surface of 111.7 km^2, 20.5% of which was affected by landslides. The spatial and temporal distribution of landslides highlighted that in several cases, they are reactivations of pre-existing phenomena. In fact, in the municipality, approximately 17% of the buildings fall within landslides-affected areas, 7.9% of which are in areas where landslides are classified as active. Furthermore, active landslides involve 8.1% and 9.5% of the roads and railways, respectively. In the 1934–2020 study period, 53% of activations occurred between October and December and were triggered by daily rain which in the highest percentage of cases (49%) showed values between 50 and 100 mm. The proposed GIS platform can be easily updated in order to preserve the landslide history of the area and can be enriched with further thematic layers (i.e., layers concerning flood events, which often occur simultaneously with major landslide events). The case study demonstrates how the platform can support landslide risk management in terms of monitoring, planning remedial works, and the realization/updating of civil protection plans.

Keywords: landslide; rainfall thresholds; geodatabase; landslide damage; Calabria

check for updates

Citation: Petrucci, O.; Scarcella, G.E.; Conforti, M. Multi-Level Data Analyses for Characterizing Rainfall-Induced Landslide Scenarios: The Example of Catanzaro Municipality (South Italy). *Water* **2023**, *15*, 2437. https://doi.org/10.3390/w15132437

Academic Editor: Ali Saeidi

Received: 30 May 2023
Revised: 26 June 2023
Accepted: 28 June 2023
Published: 1 July 2023

Copyright: © 2023 by the authors. Licensee MDPI, Basel, Switzerland. This article is an open access article distributed under the terms and conditions of the Creative Commons Attribution (CC BY) license (https://creativecommons.org/licenses/by/4.0/).

1. Introduction

Landslides are hydro-geotechnical hazards that can affect slopes situated anywhere in the world, killing people and causing damage to both natural and human-made environments. They cause huge direct damage to urban areas, farmland, and communication infrastructures, reduce pasture bio-mass production, and cause indirect damage, which can encompass all the aspects of the wellbeing of the affected communities even for long periods [1–4].

Generally, landslides are natural events connected to landscape evolution, which are influenced by a variety of geo-environmental factors such as geology, morphology, and hydrology [5,6] and are ruled by triggering mechanisms primarily related to either rain or, less frequently, earthquakes.

The present paper focuses on landslides triggered by rainfall (LTRs) where the term landslide encompasses mass movements including debris flows, soil slips, earthflows, rockslides, rock avalanches, shallow- and deep-seated slides, and complex and compound slope failures [7]. The increase in the frequency of extreme rainfall that is expected as an effect of

climate change, in conjunction with population growth, deforestation, rapid urbanization, and unplanned urban development, could cause an increasing number of damaging LTRs, with a huge socio-economic impact, especially in the most populated areas.

Based on cause–effect relationships between past landslide activations and associated rainfall records, the literature presents empirical approaches to evaluate rainfall thresholds (RTs), defined as rainfall conditions that, when reached or exceeded, are likely to trigger landslides [8]. RTs find applications in the implementation of landslide forecasting and early warning systems, and currently represent a hot topic of literature [9]: We can find papers on LTR occurring at different latitudes and in various climatic conditions, from Italy, where the study area of the present paper is located, to Taiwan [10], Asturias (NW Spain) [11], Brazil [12], and China [13], to quote only some recent studies. RTs can be extremely different in size, according to the local rainfall regimen. For example, Chiang et al. [10], for large-scale landslide areas in Taiwan, identified a rainfall threshold under controlled conditions ranging from 780 mm/day (20-year recurrence interval) to 820 mm/day (25-year recurrence interval). Bainbridge et al. [14] elaborated on an empirical antecedent precipitation (>62 mm) and intensity-duration (>10 h) threshold over which shallow landslides occur along a strategic road in Scotland. Despite the fact that empirical thresholds change according to local geomorphological and climatic conditions, they supply basic information that can be properly interfaced with different types of "local" data to provide a useful tool for the management of LTR.

Then, as mentioned, the "landslide history" of the study area covering a sufficiently long period is one of the basic ingredients for the implementation of empirical approaches for LT (landslide threshold) identification. Nevertheless, landslide history has further uses: it allows to assess the impact of landslides on the socio-economic fabric of the area and the most frequently/severely affected places, thus highlighting the phenomena to be monitored and/or destined to undergo structural works aimed at landslide risk reduction.

Official territorial agencies devoted to systematically collecting data on landslide activations are rare, as shown in a recent study that used the Historical Landslide Catalog provided by the Central Geological Survey in Taiwan [10]. In the majority of cases, data on historical landslides must be gathered from documentary sources, especially from newspapers, as are often used in research on fatalities caused by extreme events [15]. In municipal archives, documents on both slope movements and mitigation work can be found and proficiently organized into a geodatabase useful for landslide modelling to increase people's awareness of landslide risks [16]. Technical on-site inspection reports carried out by the local geological survey and disaster management authorities, combined with printed and online news, can provide a more complete landslide history and fill possible data gaps [17].

Then, the landslide history and its relationship with triggering rain supply general information on the amount of rain that, in a selected study area, can trigger landslides. Nevertheless, it is important to completely exploit documentary data, in terms of both landslide recurrence and impact. To move toward an operational risk management system, the information on LTRs and triggering rainfall must be implemented in a multi-level system containing thematic data, finalizing the knowledge framework of the study area and allowing one to correctly geo-reference landslide activations. Only with such a multi-data approach can the places affected by past landslides be labelled according to their geological-geomorphological characteristics, thus allowing an understanding of possible phenomena evolution, while the intersection of landslides with man-made elements can drive the planning of actions to reduce risk.

Due to the multiplicity of factors and the variety of data necessary for the whole treatment, this paper presents a multi-level data analysis approach to create a decision-making tool based on the systematization and exploitation of data for the management of risk induced by LTRs in populated areas. In actuality, in the study of landslides, starting with the gathering and analysis of already-available data constitutes an old and well-established rule [18] in both scientific papers and technical reports. Nevertheless, this paper

proposes a structured approach based on the implementation of a GIS platform including the most frequently available types of data (historical, geomorphological, geological, and climatic data) and suggests a procedure to take full advantage of them in light of landslide risk management. The collected data are organized in a GIS environment to guarantee easy management, analysis, updating, and sharing with different users.

The paper is structured as follows: Section 2 presents the methodological approach; Section 3 presents the study area; Section 4 describes the application of the methodology to the study area and the results obtained; Section 5 discusses the findings raised in the case study, highlighting both critical points and knowledge gaps; and finally, Section 6 presents the main conclusions.

2. Methodological Approach

We present a multi-level data analysis approach based on a GIS platform to collect various kinds of data useful for landslide risk definition and management. Figure 1 summarizes the workflow of the methodology, which is structured as three steps: data gathering, data processing, and the realization of products.

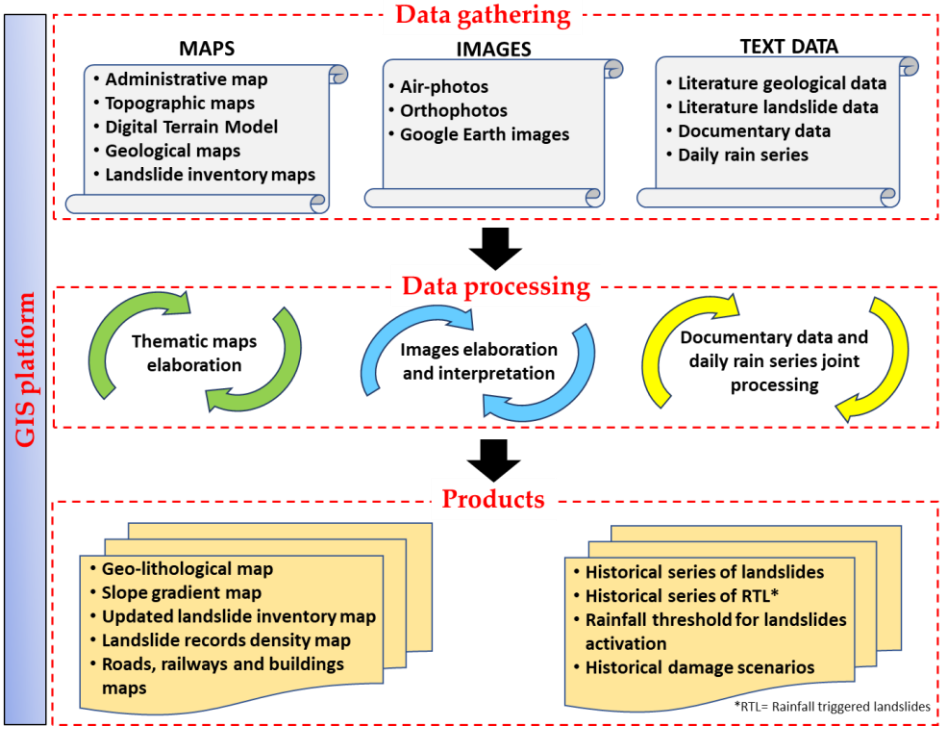


Figure 1. Flow chart of the methodological approach proposed.

2.1. Data Gathering

The methodology starts with the collection and importation of publicly available data concerning the study area (SA) into the GIS platform. The software used to realize the GIS platform is ESRI's ArcGIS ver. 10.8. According to the level of pre-elaboration required to be included in the GIS platform, we can divide data into three broad classes: maps, images, and text data (Figure 1).

Maps include both raster and vector data; in some cases, to be imported into the GIS platform, they require either a georeferentiation process or a coordinate system transformation. Using the regional administrative map, the SA can be delimitated as the one included in the boundaries of a selected municipality. Municipal boundaries, in fact, are frequently used as reference boundaries in civil protection planning and the management of emergency procedures. We propose using the municipal boundaries corresponding to LAU level 1 (Local Administrative Units), formerly NUTS level 4 in the Nomenclature of

Territorial Units For Statistics defined by Eurostat (https://ec.europa.eu/eurostat/web/nuts/national-structures, accessed on 19 January 2023).

The topographic maps, Digital Terrain Model (DTM), and geological maps represent the foundation from which the thematic maps of the SA are either extracted or elaborated. Similarly, landslide inventory maps—realized either in the framework of research works or as a result of landslide recognition carried out by risk management authorities—contain valuable information to be included in the GIS platform.

As images, the air photos, orthophotos, and Google Earth images, dating back to different years, can be used to update and complete the space–time pattern of the landslide distribution in the SA [19,20].

Text data have very different characteristics and require several purposeful pre-elaborations before they can be proficiently added to the GIS platform. Geological and landslide data from the literature are essentially accompanying reports or research papers describing the mentioned geological maps and landslide inventories; they are useful to refine the uploaded maps, even if they are not physically uploaded into the GIS.

To obtain a series of historical landslides, it must be considered that, generally, there are no agencies that officially collect landslide damage data, and documentary data analysis can make up for this lack. Among documentary data, technical and scientific reports usually describe the most destructive cases, while landslides causing low-severity damage can be obtained from the systematic analysis of daily newspapers, as widely shown in the literature on damaging hydrogeological events [21–23]. Hypothetically, the research could go back for centuries; yet, for the purpose of this study, it is necessary that it at least starts from the year in which the oldest rain gauge of the SA started to work and covers the years between that year and the present.

Daily rain data recorded at the rain gauges included in the SA are generally freely available in the form of spreadsheets from the national or regional agencies officially in charge of rainfall data collection.

2.2. Data Processing and Products

All the data stored in the GIS platform, when properly homogenized, integrated, and elaborated, allow us to produce several thematic maps and obtain useful information to understand the spatial-time distribution of landslide events. Data can either be easily merged or intersected using the geoprocessing and spatial analysis tools of ArcGIS software, to obtain new complex maps presenting several thematic layers and allow an understanding of their relationships.

The geological data are processed to prepare the geo-lithological map of the SA. From the elaboration of the DTM, by means of ArcGIS spatial analysis tools, morphometric parameters such as elevation and slope gradient can be derived. The landslide inventory maps represent a snapshot of the specific epoch in which each inventory was realized; they must be transformed into vector layers and can be combined in order to report all the landslides reported in the literature that occurred in the SA on a single map. The crosscheck analysis of all the landslide inventory maps, updated, actualized and refined using air photos, orthophotos, and Google Earth images, allows us to obtain an updated landslide inventory map of the SA.

Finally, the main human-made elements exposed to landslide risk, such as buildings and the network of roads and railways, can be easily derived from topographic maps.

The first product of the elaboration of documentary data is the historical series of landslides that affected the SA in the past. From this series, we obtain the historical series of landslides triggered by rain by simply eliminating the landslides for which phenomena descriptions did not report a clear link with rainfall, assigning their triggering, for example, to earthquakes, excavations, or water losses from pipes.

The cross-checking analysis of documentary data on LTRs and place names included in the boundaries of the SA reported on both topographic maps and Google Earth images allows us to geolocate the places affected by landslides using GIS. By means of a careful

analysis of landslide descriptions, each location affected during a certain landslide is used to create a landslide record (LR) containing the date of landslide occurrence and the site where the damage occurred. This is archived by means of the creation of a point layer, each point of which represents an LR. These data are then merged with other thematic layers and used to elaborate the density map and the spatial distribution of the historical landslide damage.

In addition, the descriptions can be used to identify what happened, in terms of damage, during historical LTRs. According to the literature [24–26], the damaged elements are sorted into the following macro-groups: roads and/or railways; buildings; people; defense work (such as retaining walls); services (such as water and electric power lines); productive activities (such as industry, commerce, or tourism); and other (to account for elements not included in previous categories). Considering the level of damage, we schematized four severity levels based on the occurrence of the following circumstances:

- LR-D1: OR mild damage to minor infrastructures and/or buildings, without people relocation, OR not specified damage.
- LR-D2: OR occurrence of minor injuries to people, AND/OR non-structural damage to infrastructures, AND/OR minor damage to buildings with brief precautionary evacuations.
- LR-D3: OR occurrence of serious injuries to people, AND/OR long-lasting structural damage to infrastructures, AND/OR prolonged public services interruption, AND/OR structural damage to buildings with prolonged evacuations.
- LR-D4: OR occurrence of fatalities, AND/OR permanent structural damage to infrastructures, AND/OR structural damage to buildings with permanent people relocation, AND/OR huge economic cost for damage retrieving.

Using these criteria, for each historical LTR, the damage scenario can be defined in terms of damaged elements and the severity level.

Finally, the joint processing of daily rain series and LTR series allows one to assess the local rainfall threshold for landslide activation. By comparing the historical series of LTR and daily rain series, we can identify the rainfall event (RE) that triggered landslides. The RE is the rain that fell between the initiation of the failure and the time when the rainfall started.

Using a literature approach, we can link the rain duration D (hours) and cumulated event rainfall E (mm), with a 5% exceedance probability, according to the power law (1) [27,28]:

$$E = (\alpha \pm \Delta\alpha) \times D^{(\gamma \pm \Delta\gamma)} \quad (1)$$

where:

- α is a scaling parameter (the intercept), assessed as 7.7.
- γ is the slope (the scaling exponent) of the power law curve, assessed as 0.39.
- $\Delta\alpha$ and $\Delta\gamma$ are the uncertainties associated with α and γ, assessed as 0.3 and 0.01, respectively.

The RE is defined as a period of continuous rain that is separated from the previous and the subsequent event by a period without rain, which is fixed to 48 h for the dry season or 96 h for the wet season [27–29]. For each rainfall event with landslides (REL), that is, one RE triggering landslide/s, the methodology assesses: (i) the duration D (hours) of the rain that presumably triggered the landslide, and (ii) the cumulated rain of the event E (mm) in the time interval D. On a logarithmic diagram, where the duration D of the REL is on the *x*-axis and the cumulated rain E is on the *y*-axis, the D-E points represent the rainfall threshold for landslide activation.

Finally, all the archived and homogenized data in the GIS environment will allow for the creation of a comprehensive landslide geodatabase to provide useful information on the spatial and temporal occurrence of landslide events, landslide sizes and types, damaged elements, damage severity level, and relationships with the geological and geomorphological features of the affected areas.

In Section 4, the practical application of the described methodology to a case study is presented.

3. The Catanzaro Study Area Framework

The SA is the territory of the Catanzaro municipality (Figure 2a), located in the central-east sector of Calabria (south Italy). This municipality has been selected for the following reasons: (a) It is representative of the problems affecting several sectors of Calabria, in terms of both geo-environmental features and landslide occurrence [19,30–32]; (b) in the peripheral framework of the region, it appears as one of the regional municipalities with the highest number of people exposed to risk. This latter condition depends on the fact that it shows a population density of 807.53 inhabitants/km^2, which is much higher than the regional average, which is equal to 127.9 inhabitants/km^2. Moreover, being the administrative regional capital of Calabria, it is crossed by a high flux of people daily coming from the entire region to interact with either the administrative offices of the region or one of the main renewed hospitals of the region and the annexed medicine faculty.

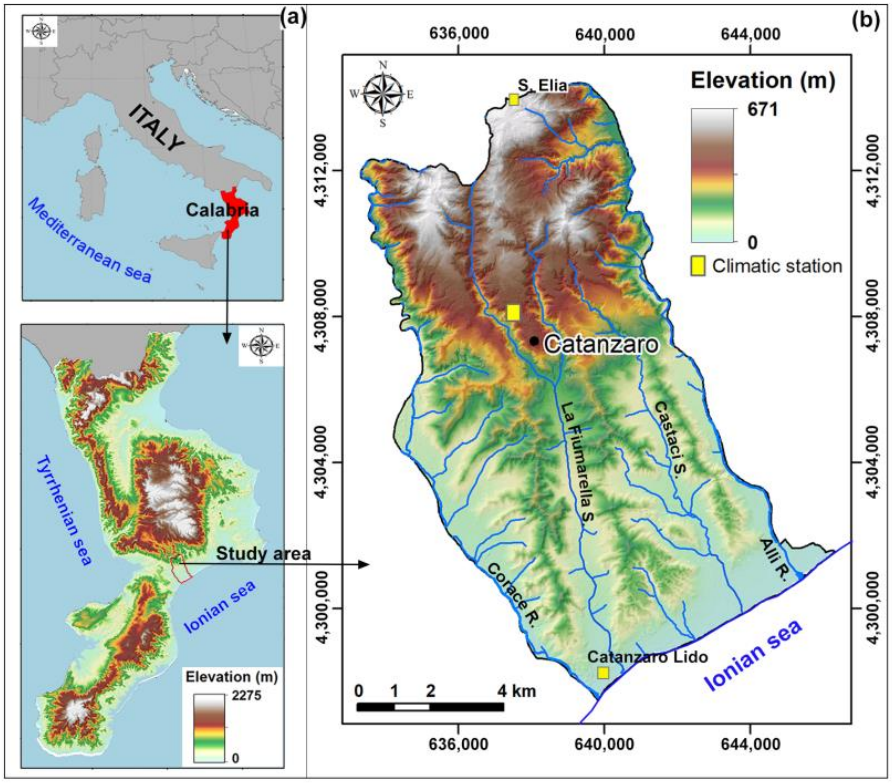


Figure 2. (**a**) Location of the study area: Calabria (top) and Catanzaro municipality (bottom); (**b**) digital elevation model of Catanzaro municipality. The locations of the climatic stations (yellow rectangles) are also reported.

The SA is allocated between 4,314,398 mN and 4,297,473 mN of latitude, and 633,322 mE and 646,315 mE of longitude, and extends over a surface of approximately 111.7 km^2. The elevation ranges from 0 to 671 m a.s.l., with an average value of 180 m a.s.l. The SA is delimited by two watercourses, both draining into the Ionian Sea: the Assi River on the left side and the Corace River on the right side (Figure 2b).

The climate is typically Mediterranean, with warm and dry summers and cold and rainy winters [33]. Rainfall data are recorded at the meteorological station of Catanzaro (4,308,080 mN, 637,504 mE, 334 m a.s.l.), located in the middle portion of the SA and currently maintained by the ARPACAL Multi-Risk Functional Centre (https://www.cfd.calabria.it/, accessed on 20 October 2022) (Figure 2b). Two further rain gauges existing in the SA cannot be utilized because they stopped working in 1998.

The mean annual rainfall is approximately 995 mm (Figure 3): generally, the rain is distributed on 90 rainy days per year, essentially between October and March, when approximately 77% of the annual precipitation falls. Generally, the rainiest months are November and December, during which several landslides occur [19,34], while June, July, and August are the driest months of the year. The maximum daily rainfall of 290 mm was registered on 16 November 1987 (Figure 3c). The mean annual temperature is 17 °C, with the mean monthly maximum in August (25.1 °C) and the mean monthly minimum in January (8.8 °C).

Comparing the trend lines of the total number of rainy days per year (Figure 3b) and the yearly rainfall intensity (Figure 3d, the ratio between total yearly precipitations and the total number of rainy days per year), we can see a clear increase in the rainfall intensity and a progressive decrease in the number of rainy days. This aspect underlines a gradual increase in short-duration high-intensity rainfall, which represents the main landslide-triggering factor, especially for soil slips [19,35].

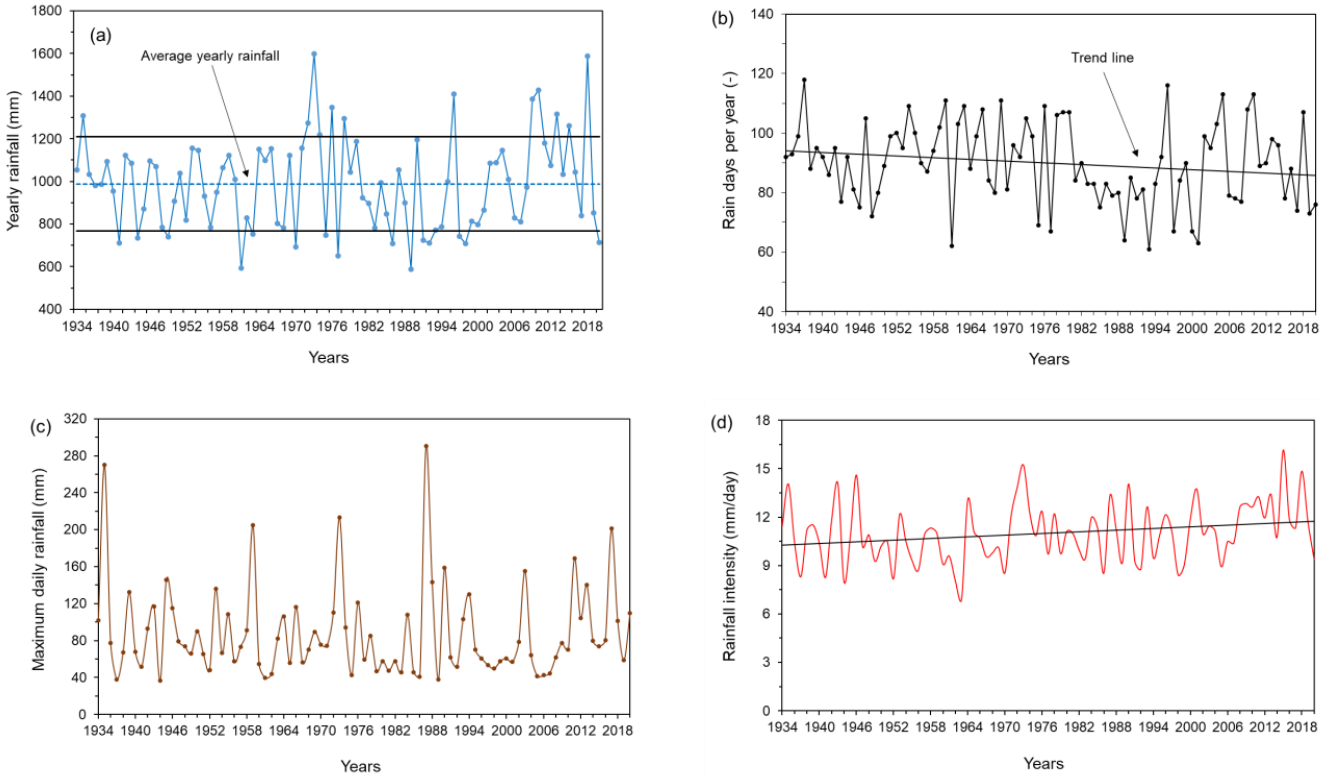


Figure 3. Some characteristics of rainfall data recorded at meteorological station of Catanzaro from 1934 to 2020; (**a**) average annual rainfall; (**b**) number of rainy days per year; (**c**) maximum daily rainfall; (**d**) rainfall intensity.

As a geo-structural setting, the SA is situated on the north-eastern edge of the Catanzaro basin (Figure 4) and is the linkage zone between the northern and southern sectors of the mountain belt named the Calabrian Arc [34,36–39]. The Catanzaro basin, including the SA, is a graben-like structure placed between Sila and Serre Massifs, bordered to the north by NW-SE-trending faults and to the south by a WNW-ESE-oriented fault system [35,38]. This basin is filled by Neogene–Quaternary sedimentary units (Figure 4) consisting of marine and continental deposits, unconformably lying on the Hercynian crystalline-metamorphic units of the Calabrian Arc [37,40,41].

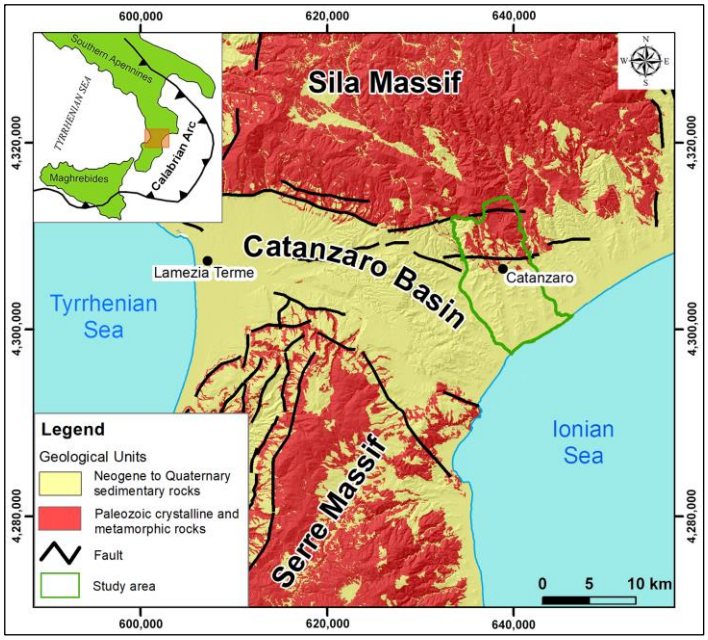


Figure 4. Geo-structural simplified sketch map of the central sector of the Calabria region.

4. Application of the Methodology to the Study Area and Results

The acquisition and incorporation in the GIS platform of the multi-source and multi-temporal data allowed a detailed characterization and mapping of the rainfall-induced landslides in the SA. The main features of the maps and images collected, and the related thematic layers obtained by means of their elaboration, are shown in Table 1.

Table 1. Characteristics of the maps and images archived in the GIS platform of the SA and related thematic maps elaborated.

Data Source	Input Format	Thematic Layer	Output Format
Regional administrative map (http://geoportale.regione.calabria.it/opendata, accessed on 10 December 2022)	Vector (polygons)	Administrative limit of study area map	Vector (polygons)
Calabria topographic map. Scale 1:5000 (http://geoportale.regione.calabria.it/opendata, accessed on 10 December 2022)	Vector (points, lines & polygons)	- Road and railway network map - Building map	Vector (lines & polygons)
Calabria DTM. Pixel size 5 m (http://geoportale.regione.calabria.it/opendata, accessed on 15 December 2022)	Raster	- Elevation map - Slope gradient map	Raster
Calabria geological map. Scale 1:25,000 (http://geoportale.regione.calabria.it/opendata, accessed on 27 May 2021)	Vector (polygons)	Geo-lithological map	Vector (lines & polygons)
ITHACA Catalogue (http://sgi1.isprambiente.it/geoportal/catalog/main/home.page, accessed on 12 June 2021)	Vector (lines)		
Catanzaro strait litho-structural and landslide map. Scale 1:50,000 [34]	Raster		
Landslide inventory map by Calabria Basin Authority (Piano di Assetto Idrogeologico—Law 267/98, updated in 2016) (http://geoportale.regione.calabria.it/opendata, accessed on 10 April 2019)	Vector (polygons)		

Table 1. *Cont.*

Data Source	Input Format	Thematic Layer	Output Format
Map of shallow landslides triggered by rainfall in Catanzaro strait. Scale1:10,000 [19]	Raster	Updated landslide inventory map	Vector (polygons)
LiDAR-DTM, Italian Ministry for the Environment, Land and Sea, 2012. Pixel size: 1 m (http://wms.pcn.minambiente.it, accessed on 24 October 2021)	Raster		
1954 and 1990 air-photos. Scale 1:33,000 (Italian Military Geographical Institute—IGMI)	Raster		
Calabria orthophotos (2007). Scale 1:10,000 (http://geoportale.regione.calabria.it/opendata, accessed on 19 July 2019)	Raster		
Google Earth satellite images dated: 2009, 2010, 2011, 2014, 2016, 2019, and 2020	Raster		

4.1. Geo-Lithological and Geomorphological Analysis

By integrating and elaborating on the pre-existing geological and structural data (Table 1), the geo-lithological map of the SA was generated (Figure 5a). In the north sector of the SA, Paleozoic intrusive and metamorphic rocks (gneiss, schist, and phyllite) represent the Sila Massif basement outcrop [39]. Fracturing and severe chemical-physical weathering processes produced the degradation of these rocks, which are often mantled by thick regolith horizons [42,43]. In this sector, evaporitic and conglomeratic Miocenic sequences unconformably lie over the Paleozoic bedrock [44]. Locally, an alternation of weak sandstone and Pliocene sands also outcrop (Figure 5a). Moving to the southern sector, Pliocene deposits, primarily made of silty clays and occasionally interbedded by weak sandstones and sands, cover the mentioned Miocene terrigenous sediments. Along the coastal area, the top of the sedimentary succession is constituted by marine terraced deposits, compounded by conglomerates and sands of the Pleistocene. Finally, Holocene alluvial deposits are present along both valley floors and the coastline; also, along the latter, beach sediments can be found. The northern and central sectors of the SA are crossed by several normal faults, with an average N 120° trend [34,36] (Figure 5a).

The morphological features of the SA are clearly linked to the variety of outcropping lithologies and the structural setting. According to the hardness of the lithologies, the slope gradients range between 0 and 73°, with an average of 14.6° (Figure 5b). The upper sectors, made of Paleozoic rocks and Miocene deposits, are affected by instability phenomena and present a rugged morphology with deep-cut valleys and slope gradients of up to 40° [19,32]. Flat or gently sloping summit surfaces, often bordered by steep slopes and dissected by deep gullies, also occur. Moreover, tectonic-originated fault-controlled landforms, such as morpho-structural ridges bounded by fault scarps and morpho-structural alignments, also appear.

Central and lower sectors, primarily made of silty-clayey deposits, show a hilly landscape with undulating morphology, rounded slopes, and wide slightly incised valleys (Figure 5a). Along the coast, stream dissection originates, gently to moderately dipping homoclinal ridges in clastic successions, onto which relict limbs of stepped surfaces occur. These surfaces, locally forming SE-striking staircase landforms along the interfluve ridges, are remnants of marine terraces created by the interference between tectonics, the climate, and sea-level changes. Silty-clayey hillslopes locally show badlands, with a pinnate drainage network and steep gullies separated by narrow and knife-edged crests [19,45].

The present-day landscape evolution is essentially controlled by both landslides and either diffuse or linear runoff processes [8,20,21,46,47].

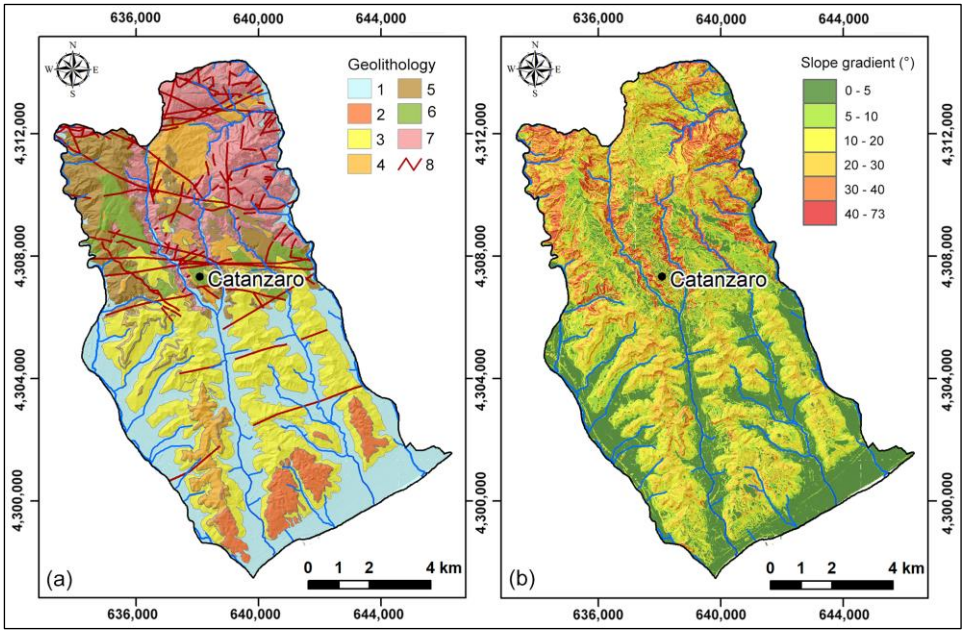


Figure 5. (**a**) Geo–lithological map of the Catanzaro municipality: (1) Alluvial deposits (Holocene), (2) sand and conglomerate deposits (Pleistocene), (3) silty clay deposits (Pliocene), (4) weak sandstone and sand (Pliocene), (5) conglomerates (Miocene), (6) evaporitic and limestone deposits (Miocene), (7) intrusive and metamorphic rocks (Paleozoic), (8) fault; (**b**) slope gradient map.

4.2. Updated Landslide Inventory Map

A careful geomorphological recognition, addressed to recognize geometry, activity state, and type of landslides according to the classification by Cruden and Varnes (1996) [18], was performed to create an updated landslide inventory map based on the integration of:

- Stereoscopic analysis of aerial photographs dated 1954 (the oldest aerial photographs in this area) and 1990, respectively.
- Visual analysis of orthophotos dated 2007.
- Visual analysis of Google Earth images of the period 2009–2021.
- Visual interpretation of thematic maps (slope gradient, hillshade, and contour lines) produced by the DTM (pixel size: 1 m) deriving from LiDAR scanning on an aerial platform acquired in 2012 by the Italian Ministry for the Environment, Land, and Sea (http://wms.pcn.minambiente.it, accessed on 24 October 2021).
- Landslide inventory carried out by the Regional Basin Authority (Piano di Assetto Idrogeologico—Law 267/98) adopted in 2001 and updated in 2016 (http://geoportale.regione.calabria.it/opendata, accessed on 10 April 2019).
- Field investigations carried out in several stages throughout the last three years.

In addition, important information was gathered from literature data, essentially from previous studies conducted for research purposes [8,21,23,48].

All the collected data were digitized (the landslides were digitized as polygons comprising scarp and deposit areas) and uploaded into the GIS platform to obtain an updated landslide inventory map representing a quite complete sketch of the landslide's spatial distribution (Figure 6). It shows that both deep-seated and shallow landslides, with different sizes and states of activity, are widespread in the SA. As a whole, 487 landslides, representing an average density of approximately 4.4 landslides per square kilometer, were mapped (Table 2). As far as the type of movement, 225 landslides (46.2%) were classified as slides, 30 (6.2%) as flows, and 93 (19.1%) as complex phenomena. The geomorphological survey also highlighted several gentle slopes carved in silty clay sediments affected by slow and superficial slope deformations, such as soil creep, especially on agricultural lands. The term shallow-landslide area has been used to indicate: (i) unstable areas where the clustering of landslides was so tight that it was impossible to distinguish different bodies, and (ii) numerous small phenomena very close to each other

and too small to be mapped. These kinds of mass movements cover a considerable portion of the SA, especially in clayey deposits, and primarily consist of slide-flow phenomena. Landslide size varied from 1.62×10^2 to 135.51×10^4, with a mean value of 46.93×10^3 (Table 2). Overall, mapped landslides cover an area of 22.9 km^2, which represents 20.5% of the SA.

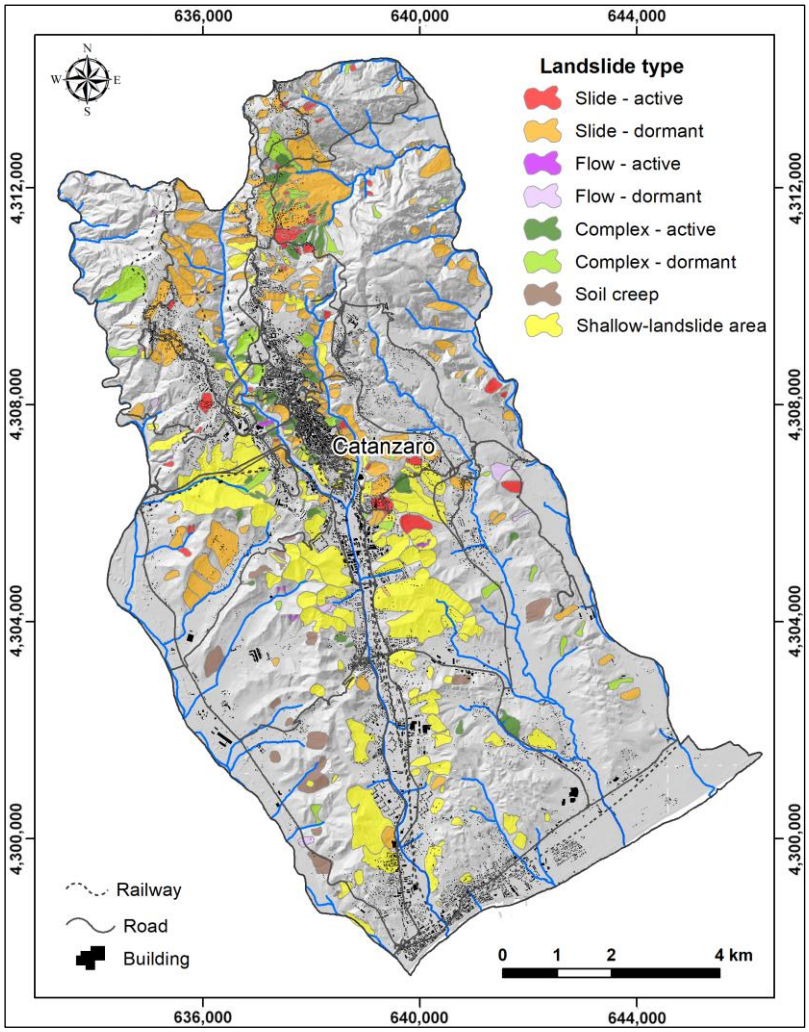


Figure 6. Landslide inventory map of Catanzaro municipality.

Table 2. Landslide data for Catanzaro municipality derived from the inventory.

	Slide	Flow	Complex	Soil Creep	Shallow-Landslide Area	Total
Tot. area (km^2)	n/a	n/a	n/a	n/a	n/a	111.7
Tot. number of landslides	225	30	93	17	122	487
Type of landslide (%)	46.2	6.2	19.1	3.5	25.1	100.0
Tot. area affected by landslides (km^2)	8.5	0.5	3.0	1.0	10.1	22.9
Tot. area affected by landslides (%)	7.6	0.4	2.7	0.9	9.0	20.5
Landslide density (landslide/km^2)	2.0	0.3	0.8	0.2	1.1	4.4
Area of the smallest landslide (m^2)	1.39×10^2	5.81×10^2	8.73×10^2	5.81×10^3	8.87×10^2	1.39×10^2
Area of the largest landslide (m^2)	103.43×10^4	86.56×10^3	396.27×10^3	149.69×10^3	135.51×10^4	135.51×10^4
Average landslide area (m^2)	37.57×10^3	12.06×10^3	31.85×10^3	57.31×10^3	82.85×10^3	46.93×10^3

Multi-temporal aerial photo interpretation and field surveys provided data to distinguish between active (38%) and dormant (62%) landslides. Moreover, both the soil creep and shallow landslide areas were considered active, thanks to their morphological evidences suggesting seasonal reactivations.

The inventory map (Figure 6) highlights that a large number of landslides were mapped on the foothill slopes of the Sila Massif and along the hillslopes surrounding the Catanzaro urban center. Several phenomena appear to be concentrated along the faults, representing weakness zone predisposing deep weathering processes [34]. Moreover, in the central sector, the hillsides carved on clayey terrains, even with low-gradient slopes, are affected by widespread landslides, primarily shallow landslides and soil creep. In contrast, alluvial and coastal plains are rarely affected by instability phenomena. Thus, the landslide spatial distribution suggests that their occurrence is strictly controlled by lithology, tectonic setting, and morphometric features [49].

The overlapping of the landslide inventory map and the geo-lithological map reveals silty clay and weathered intrusive and metamorphic rocks as the most affected by landslides, followed by weak sandstone, sand, and conglomerate (Figure 7a). Thus, by defining the landslide index as the ratio in percentage between the landslide area and total area in each lithological class, the mentioned lithologies show the highest landslide indexes of the SA.

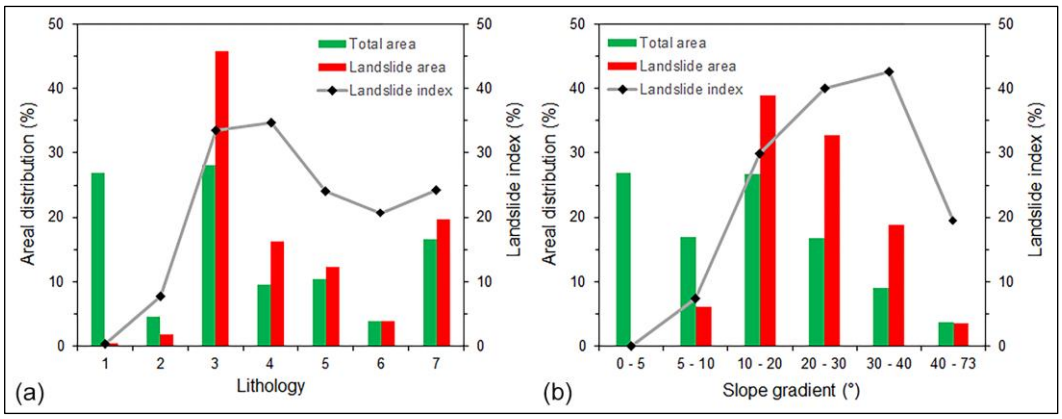


Figure 7. Distribution of total area, landslide area, and landslide index for the (**a**) lithology types (1. alluvial deposits (Holocene), 2. sand and conglomerate deposits (Pleistocene), 3. silty clay deposits (Pliocene), 4. weak sandstone and sand deposits (Pliocene), 5. conglomerate deposits (Miocene), 6. evaporite limestone deposits (Miocene), and 7. intrusive and metamorphic rocks (Paleozoic); (**b**) slope gradient classes.

Moreover, several landslides are highly linked to structural features because the faults have caused intense fracturing and deformation of the rocks, high local relief, and fluvial undercutting. In some cases, landslide occurrence is related to stratigraphic/tectonic contact between more and less competent sequences, with severe rock weathering reducing the shear strength [48,49].

The slope gradient is considered the main morphometric factor influencing slope instability [49], as the shear stress increases with an increasing slope gradient. The comparison between the slope gradient map, sub-divided into six classes (0–5°, 5 –10°, 10–20°, 20–30°, 30–40°, and >40°), and the landslide inventory revealed that the landslide abundance gradually increases with the increase in the slope gradient, up to slope values of 40 degrees. Above this value, instability phenomena generally decrease (Figure 7b). In the majority of landslides (approximately 72%), the slope gradient values fall in the range of 10–30 degrees. In terms of the landslide index, higher values were observed for the classes 20–30° (44.4%) and 30–40° (42.6%) (Figure 7b).

4.3. Historical Rainfall-Induced Landslide Geodatabase

The first step was to identify historical landslides affecting the SA over the years and build the landslide geodatabase. The historical data used in this paper were obtained from ASICal (Italian acronym for historically flooded areas), a catalogue containing flood and landslide damage occurring in the Calabrian region since the end of 1800 [50], already exploited in several papers concerning either past landslides [29] or floods [51]. As they are data obtained from documentary sources, their time resolution is daily: The day of landslide occurrence is available for all cases, while the hour is quoted only in a few cases. As is widely known in the literature, catalogues that can be obtained from documentary sources only include landslides that cause certain damage, especially human losses [52–54]. Generally, phenomena that did not cause damage, for example, landslides that occurred in unpopulated areas, are not reported by documentary sources.

The first landslide damage record in the SA dates back to 1934. By means of a careful analysis of LE descriptions, each location affected during a certain LE was used to create a landslide record (LR), containing information about the date of occurrence and the site where landslide damage occurred.

Data from the ASICal database, complemented with further historical research, allowed us to identify 88 LEs, which affected the SA in the period of 1934–2020. These 88 LEs have led to the recognition of 277 LRs (Figure 8). In 52% of cases, the Les has a widespread effect on the SA, with the simultaneous triggering of landslides in different sectors labelled by relative toponyms, while in the remaining 48% of cases, landslide effects were more localized and limited to a single site. On average, the number of LRs per LE is 3, while the highest number of LRs (equal to 16) concerns LEs in 1972 and 1993 (Figure 8a).

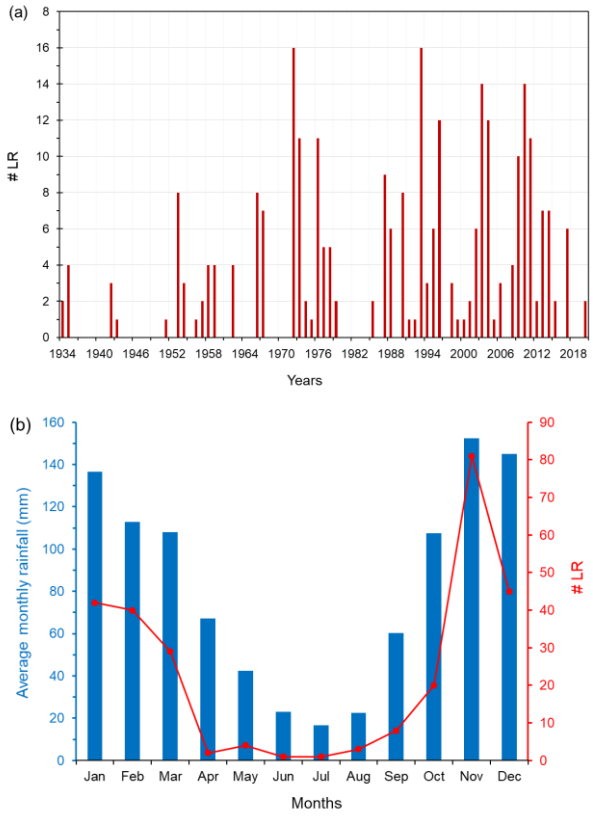


Figure 8. (**a**) Number of landslide records (#LR) per year in the period of 1934–2020; (**b**) monthly average rainfall and number of landslide records that occurred from 1934 to 2020.

In the SA, numerous landslide events occur in the period from November to March (Figure 8b); specifically, 53% of LRs were recorded in the months between October and December, 40% between January and March, and only 7% occurred in the period from April to September. Analyzing triggering rainfall, 6% of LEs (occurring in 1935, 1959, 1973, 1987, and 2017) recorded maximum daily rain exceeding 200 mm, 14% of LEs (occurred in 1934, 1957, 1967, 1975, 1991, 1992, 1995, 2001, 2004, 2006, 2009, and 2014) recorded daily rain between 40 and 50 mm, and the remaining 80% of cases show values ranging between these two extremes, with the highest percentage (49%) between 50 and 100 mm.

We investigated the temporal and seasonal distribution of the LRs in three sub-periods [29]: 1934–1964, 1965–1994, and 1995–2020 (Table 3). We observed an increase in the LRs during this time: 14% of LRs occurred in the first period, 41% in the second period, and 45% in the last period. This can be justified by the lack of information sources in the older period with respect to the most recent years.

Table 3. Mean rainfall intensity (MIR) and distribution of LRs in the three periods (1934–1964, 1965–1994, and 1995–2020) and in the entire period (1934–2020) for each season.

Period	1934–1964		1965–1994		1995–2020		1934–2020	
	MIR (mm/gg)	LRs (#)	MIR (mm/gg)	LRs (#)	MIR (mm/gg)	LRs (#)	MIR (mm/gg)	LRs (#)
Winter	10	10	11	41	12	60	11	111
Spring	8	0	8	4	9	4	8	8
Summer	10	0	11	2	12	10	11	12
Autumn	12	27	13	67	13	52	13	146
Yearly	11	37	11	114	12	125	11	276

Concerning the seasonal distribution, in the oldest period, more than 70% of LRs occurred in autumn and winter, while, in the other periods, winter LRs increased and spring and summer slightly increased too. As far as the temporal distribution, by comparing the average rainfall intensity (the ratio between the average rainfall and the average number of rainy days for all years of each period), we can see an increase in the rainfall intensity over time that underlines the variation of the LR distribution in the different periods analyzed.

Using topographic maps and Google Earth images, the sites where LRs occurred were identified and mapped as points (Figure 9a). Each point is complemented with a series of attributes: The landslide event record identifier; the place name; coordinates; year, month, and day of the landslide occurrence; the type of landslide; the damaged elements; and a textual field containing the original description of the landslide, as gathered from the data source. The collected data allowed the construction of an LR density map (Figure 9a), created by means of the kernel density algorithm with spatial resolution of 5 m and radial search area of 1 km^2, using ESRI ArcGIS 10.8 software. The LR density represents the number of LRs per square kilometer that occurred during the study period. The map highlights the sectors of the study area characterized by different concentrations of LRs: LR density ranges from 0 to 36 LRs/km^2, with 2.7 LRs/km^2 as the mean value. Particularly, high LR density characterizes the hamlets of Pontegrande and S. Elia, and the urban center of Catanzaro (Figure 9a).

Finally, by comparing the landslide inventory map with the geo-localization of LRs, we observed that, during the study period (1934–2020), several LRs concern the same sites, thus representing multiple reactivations of the same landslide [32]. For example, in the Pontegrande hamlet, we mapped several active landslides that showed activations in 1966, 1973, 1976, 1988, 1996, and 2010 (Figure 9b).

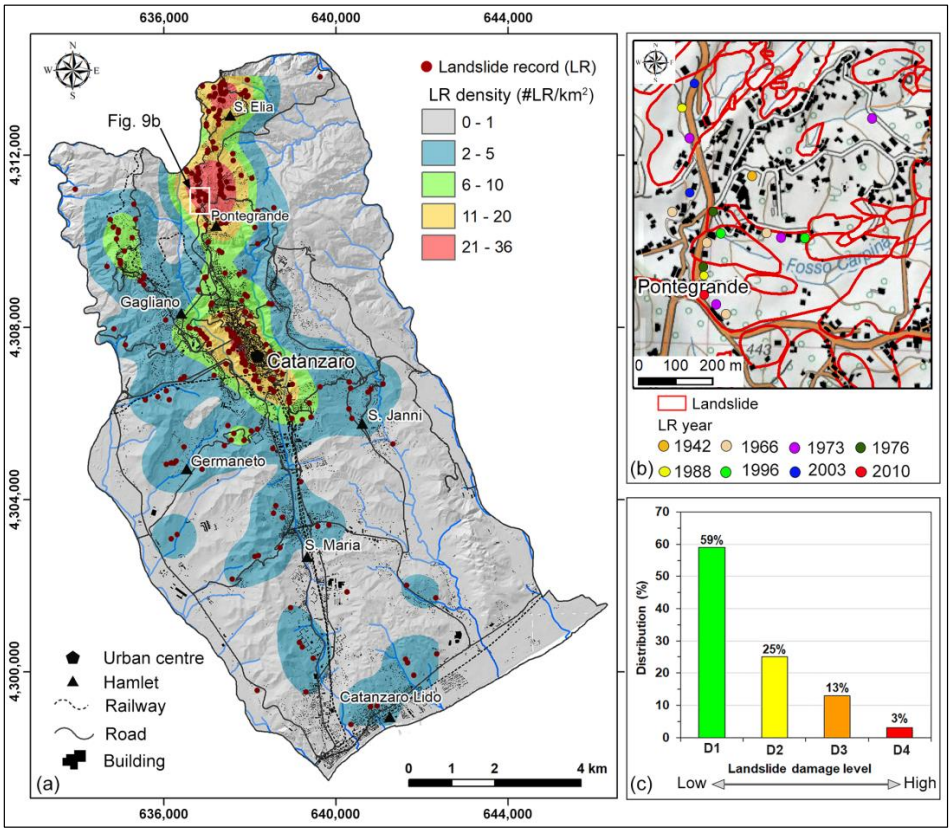


Figure 9. (**a**) Geo–localization of each landslide record (LR) and LR density map of Catanzaro municipality; (**b**) example of multiple reactivations of the same landslide; (**c**) distribution of different landslide damage levels.

4.4. Landslide Rainfall Threshold

By comparing LE occurrences with the rainfall records of the Catanzaro climatic station we identified 66 rainfall events with landslides and discarded 22 landslide events not strictly related to rainfall (daily rain preceding LEs was absent or less than 10 mm). Thus, we performed the application of the national rainfall threshold developed by Peruccacci et al. [28] to the 66 RELs, assessing the duration D (h) of the triggering rain and the cumulative precipitation of the event E (mm) at the time D. The D-E points of 66 RELs are reported in Figure 10.

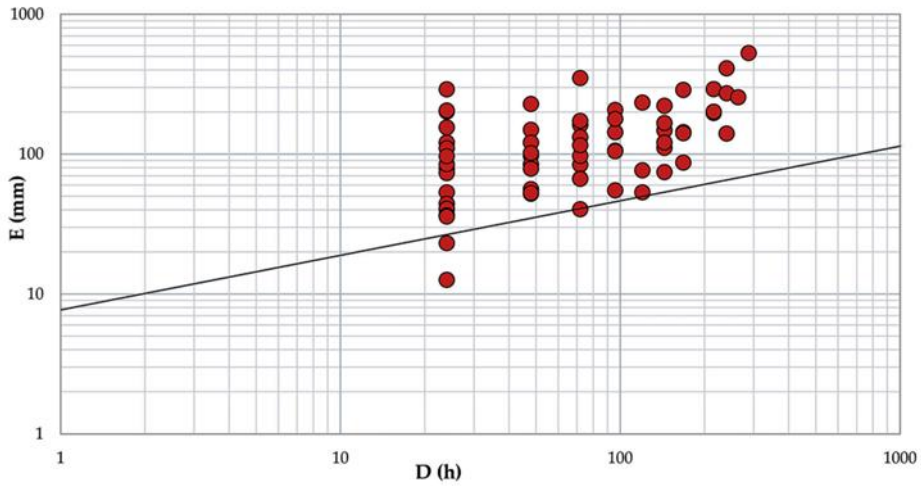


Figure 10. Results of the application of national landslide triggering threshold [28]. Data are shown in log-log coordinates.

The validation of the results was carried out by comparing the E-D values recorded during RELs with the national threshold. Based on the exceedance/not exceedance of the rainfall national threshold, we identified (a) 64 RELs that exceeded the threshold (points above the threshold line) and (b) 2 RELs that did not exceed the threshold (points below the threshold line, occurring in February 1954 and December 1995). This highlights a good level of performance of the methodology, with only 5% of the cases under the threshold. Thus, the rainfall threshold applied is able to discriminate the RELs and consequently to identify the probability of occurrence of rainfall-induced landslides in the SA.

4.5. Landslide Damage Scenarios

The analysis of historical documents enabled us to obtain information about the damaged elements and severity of landslides damage that frequently affected both social and economic activities, as well as structures and infrastructure networks. Roads and/or railways, with 44% of cases, were the most frequently damaged elements, followed by buildings, with 25% of cases (Figure 11). The constant landslide threat to roads depends firstly on the road path (often crossing landslide-prone areas) and secondly on the instabilities of the road cuts realized to create the path for road construction. In 8% of cases, people were among the damaged elements, particularly the events that occurred in November 1935 (three fatalities) and November 2011 (one fatality).

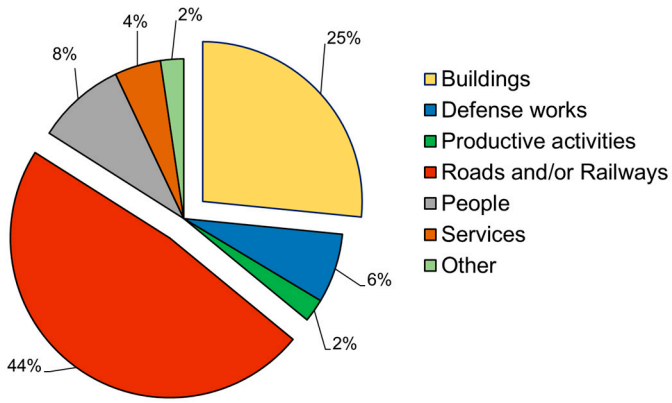


Figure 11. Elements damaged by landslide events (percentage of cases).

As far as the severity of the damage, only in a few cases (3%) was the highest level of damage severity (D4) recorded, while the majority of cases (59%) caused low-severity damage (D1) and the remaining cases had damage levels of D3 (13%) and D2 (25%) (Figure 9c).

Using a GIS-based spatial analysis, implemented in ArcGIS software, the evaluation of the structures and infrastructures involved in landslides was performed by means of the geometric intersection between the landslide inventory map, the road and railway network, and building layers. The GIS intersection allowed us to outline the roads, railroads, and buildings damaged by landslides (Table 4).

Landslides damaged several sections of both road and railway networks, causing the blockage of traffic and consequent socio-economic inconvenience to the people who use these infrastructures daily. Specifically, 14.9% (12.1 km) of roads and 17.8% of railways are affected by landslides, and active landslides involve 8.1% and 9.5% of the roads and railways, respectively (Table 4).

The geometric intersection between the landslide inventory map and building layers showed that 2062 buildings (17% of the total) fall within areas affected by landslides several of which (7.9%) concern active landslides (Table 4), thus exposing people to high-risk conditions.

Particularly, the urban center of Catanzaro and the hamlet of Pontegrande were the sectors most frequently affected by landslide activations or re-activations, causing huge damage to roads, railways, and buildings (Figure 9a). Multi-temporal analysis revealed that some roads and buildings were realized within pre-existing landslides, thus exposing

these man-made elements to landslide hazards. These findings highlight the need to draw the attention of land managers to the impact of landslides on infrastructures and structures.

Table 4. Elements damaged by landslides.

Typology	Total	Affect by Landslides		
		Active	Dormant	Total
Roads (km)	149.8	12.1 (8.1%)	10.2 (6.8%)	22.3 (14.9%)
Railways (km)	39.9	3.8 (9.5%)	3.3 (7.5%)	7.1 (17.8%)
Buildings (#)	12,151	957 (7.9%)	1105 (9.1%)	2062 (17%)

5. Discussion

Certain key features concerning the data used in our approach need to be addressed. The first is the time and effort required to build an accurate and sufficiently long catalogue of historical landslides, depending on both the abundance of data sources and the skill of investigators. Secondly, our catalogue only includes landslides that were recorded in documentary sources because they have "caused some damage" to either properties or the population. Thus, this catalogue does not include landslides that did not cause damage, but we maintain that it can be considered a complete catalogue in time and space concerning damaging landslides in the SA. After all, the approach is proposed to facilitate landslide risk management, and thus it is focused only on those landslides that could interact with people and/or goods and become a source of risk. Third, an underestimation in the number of landslides occurred in the oldest years of the series can be supposed, but this cannot be fixed due to the low availability of the sources of information of that time, especially if compared to the current data availability.

Moving to rainfall data, the main problem is related to the availability of data collected systematically for a long period and without gaps from some kind of accredited body. This means that the analysis is conditioned by the presence of rain gauges continuously working in the study area. In actuality, for our case study, we could only count on a single gauge because the other two existing in the area were not continuously working. Moreover, in light of the integration of different types of data for landslide risk definition, it must be taken into account that the density of rain gauges can affect LT results, especially in mountainous territories, because the representativeness of measured rain depends on the distance between the rain gauge and the landslide. Finally, the daily time scale of the rainfall series used to assess LT might not be the best time scale to cope with landslides, particularly shallow landslides. It is not adequate for identifying rainfall thresholds for sub-daily duration events, and thus the thresholds defined cannot be used in landslide warning systems, even if they are adequate to detect variations in the landslide-triggering rainfall conditions in the study area.

The application of the proposed approach allowed us to put together all the elements contained in the gathered data and add the additional information originating from the data spatial analysis and cross-checking. All types of data utilized are widely used in the management of landslide risk, and the main point of weakness of the methodology could be the lack of novelty. Nevertheless, the novelty of this approach is more in the way in which data are gathered and organized, obtaining the series of advantages described in the following points.

The realization of such a GIS platform following a progressive structured approach and driving the realization of well-defined products ensures the possibility of collecting, exploiting, and updating all the data available on landslide occurrence in a SA.

The point GIS layer allowing the georeferenced use of documentary data on past landslide activations ensures the identification of affected places and damaged elements and can be improved if further data on past events become available. Moreover, the GIS can be maintained and even updated in the case of future landslide occurrences by simply introducing new landslides (or landslide reactivations) both in the updated landslide inventory map and in the point layer of affected sites.

The simple and schematic description of the steps to apply the methodology ensures its utility even outside the research field, especially in the more technical and operational dimension of risk management in small territorial frameworks such as municipalities, at the scale of which the study was customized. In this applicative framework, the GIS supply certified evidence of the more frequently damaged sites and their relationships with triggering rainfall thresholds, combined with typical damage scenarios occurring in the area and useful for local authorities to plan emergency management.

The prediction of rainfall conditions that may lead to landslides, obtained based on the literature approach, may be relevant to plan the management of multiple landslide-triggering events leading to critical emergency conditions. Nevertheless, it must be taken into account that the level of accuracy of the data can bias the threshold's affordability. The experience showed that the occurrence of a landslide could not fully be reflected in documentary sources: Landslides causing social or economic impact are generally reported, while the remaining failures go unreported or are reported without any spatial or temporal reference, and this can affect the spatial data homogeneity. Despite being widely known in the literature, these problems cannot be completely fixed because "official" databases of landslide activation are rare and often obtained using only newspaper collections. Due to their daily cadence, newspapers are the most used data source, allowing systematic day-by-day screening over long periods.

Further improvements should be the realization of specific research on structural works realized over the years and the creation of a new specific section structured to collect the large variety of types of data included in the relative projects. Other thematic layers, particularly concerning the effects of floods occurring in the same study period, can give indications for the management of geo-hydrological risk in the SA.

Finally, the data collected in the GIS platform coupled with spatial analysis techniques allows multi-layer analysis, which can be used in the zonation of landslide risk.

6. Conclusions

We presented a multilevel data system, in the GIS environment, that can become an important tool of knowledge for the landslide risk management of small territorial units as municipalities. It does not require expensive field surveys because it is designed to benefit from all of the already-available data collected for different purposes, either in research or technical frameworks.

To demonstrate the use of the methodology, we analyzed the landslide risk in the municipality of Catanzaro (southern Italy), having a surface of 111.7 km^2, 20.5% of which is affected by landslides, either active (38%) or dormant (62%). In the study period of 1934–2020, 52% of landslide events had a widespread effect on the municipal area. The rugged upper sectors (671 m a.s.l.), made of Paleozoic rocks and Miocene deposits, are the most densely populated and most frequently affected by instability phenomena. The majority of activations (53%) occurred between October and December and were triggered by daily rain that, in the highest percentage of cases (49%), ranged between 50 and 100 mm.

Approximately 17% of the buildings existing in the SA fall within landslide-affected areas, and 7.9% are located in areas in which landslides are classified as active. Active landslides affect 8.1% and 9.5% of the roads and railways, respectively. The first zonation of sectors more affected by landslides is presented in the landslide records density map.

Considering the widespread diffusion of landslides throughout the 86-year study period and the relatively low value of daily rain able to trigger instabilities, a multi-level data system represents a support to (a) plan the emergency management in cases of simultaneous occurrence of landslides on various sectors of the municipal territory, (b) identify phenomena to be monitored, (c) intensify monitoring systems on phenomena that can block traffic on roads and railways, (d) prioritize phenomena to be undertaken to structural works for landslide risk reduction, and (e) realize/update civil protection plans. A test of the landslide threshold and the global operability of the platform should be planned for the next autumn–winter season. The proposed GIS platform can be easily updated in order

to preserve the landslide history of the area and can be enriched with further thematic layers (i.e., layers concerning flood events, which often occur simultaneously with major landslide events).

Author Contributions: Conceptualization, O.P. and M.C.; investigation and data processing, G.E.S. and M.C.; spatial analysis and data curation, G.E.S. and M.C.; writing—original draft preparation, M.C.; writing—review and editing O.P. All authors have read and agreed to the published version of the manuscript.

Funding: This work was funded by the Next Generation EU—Italian NRRP, Mission 4, Component 2, Investment 1.5, call for the creation and strengthening of 'Innovation Ecosystems', building 'Territorial R&D Leaders' (Directorial Decree n. 2021/3277)—project Tech4You—Technologies for climate change adaptation and quality of life improvement, n. ECS0000009. This work reflects only the authors' views and opinions, neither the Ministry for University and Research nor the European Commission can be considered responsible for them.

Data Availability Statement: The data presented in this study are available upon request.

Acknowledgments: Historical landslide data and rainfall thresholds assessment are part of G. E. Scarcella's thesis "Geodatabase of landslide events in the Catanzaro municipalities and rainfall analysis" for the Master "Multi-risk analysis and civil protection planning", edition 2021–2022, organized by CAMILab of Department of Informatics, Modelling, Electronics, and System Engineering of the University of Calabria.

Conflicts of Interest: The authors declare no conflict of interest.

References

1. Badoux, A.; Andres, N.; Techel, F.; Hegg, C. Natural Hazard Fatalities in Switzerland from 1946 to 2015. *Nat. Hazards Earth Syst. Sci.* **2016**, *16*, 2747–2768. [CrossRef]
2. Borden, K.A.; Cutter, S.L. Spatial Patterns of Natural Hazards Mortality in the United States. *Int. J. Heal. Geogr.* **2008**, *7*, 64. [CrossRef] [PubMed]
3. Froude, M.J.; Petley, D.N. Global Fatal Landslide Occurrence from 2004 to 2016. *Nat. Hazards Earth Syst. Sci.* **2018**, *18*, 2161–2181. [CrossRef]
4. Petrucci, O. Landslide Fatality Occurrence: A Systematic Review of Research Published between January 2010 and March 2022. *Sustainability* **2022**, *14*, 9346. [CrossRef]
5. Ma, K.; Ren, F.; Huang, H.; Yang, X.; Zhang, F. Experimental Investigation on the Dynamic Mechanical Properties and Energy Absorption Mechanism of Foam Concrete. *Constr. Build. Mater.* **2022**, *342*, 127927. [CrossRef]
6. Ma, K.; Liu, G. Three-Dimensional Discontinuous Deformation Analysis of Failure Mechanisms and Movement Characteristics of Slope Rockfalls. *Rock Mech. Rock Eng.* **2022**, *55*, 1–22. [CrossRef]
7. Hungr, O.; Leroueil, S.; Picarelli, L. The Varnes Classification of Landslide Types, an Update. *Landslides* **2014**, *11*, 167–194. [CrossRef]
8. Guzzetti, F.; Peruccacci, S.; Rossi, M.; Stark, C.P. The Rainfall Intensity-Duration Control of Shallow Landslides and Debris Flows: An Update. *Landslides* **2008**, *5*, 3–17. [CrossRef]
9. Segoni, S.; Piciullo, L.; Gariano, S.L. A Review of the Recent Literature on Rainfall Thresholds for Landslide Occurrence. *Landslides* **2018**, *15*, 1483–1501. [CrossRef]
10. Chiang, J.L.; Kuo, C.M.; Fazeldehkordi, L. Using Deep Learning to Formulate the Landslide Rainfall Threshold of the Potential Large-Scale Landslide. *Water* **2022**, *14*, 3320. [CrossRef]
11. Valenzuela, P.; Zêzere, J.L.; Domínguez-Cuesta, M.J.; Mora García, M.A. Empirical Rainfall Thresholds for the Triggering of Landslides in Asturias (NW Spain). *Landslides* **2019**, *16*, 1285–1300. [CrossRef]
12. Ehrlich, M.; Luiz, B.J.; Mendes, C.G.; Lacerda, W.A. Triggering Factors and Critical Thresholds for Landslides in Rio de Janeiro-RJ, Brazil. *Nat. Hazards* **2021**, *107*, 937–952. [CrossRef]
13. Hou, J.; Dou, M.; Zhang, Y.; Wang, J.; Li, G. An Evaluation Model for Landslide and Debris Flow Prediction Using Multiple Hydrometeorological Variables. *Environ. Earth Sci.* **2021**, *80*, 515. [CrossRef]
14. Bainbridge, R.; Lim, M.; Dunning, S.; Winter, M.G.; Diaz-Moreno, A.; Martin, J.; Torun, H.; Sparkes, B.; Khan, M.W.; Jin, N. Detection and Forecasting of Shallow Landslides: Lessons from a Natural Laboratory. *Geomat. Nat. Hazards Risk* **2022**, *13*, 686–704. [CrossRef]
15. Brázdil, R.; Chromá, K.; Dolák, L.; Zahradníček, P.; Řehoř, J.; Dobrovolný, P.; Řezníčková, L. The 100-Year Series of Weather-Related Fatalities in the Czech Republic: Interactions of Climate, Environment, and Society. *Water* **2023**, *15*, 1965. [CrossRef]
16. Notti, D.; Guenzi, D.; Lasaponara, R.; Giordan, D. Merging Historical Archives with Remote Sensing Data: A Methodology to Improve Rockfall Mitigation Strategy for Small Communities. *Land* **2022**, *11*, 1951. [CrossRef]

17. Kumari, S.; Chaudhary, A.; Shankar, V. Modelling of Rainfall Threshold for the Initiation of Landslides in Lesser Himalayan Region Using THRESH. *Model. Earth Syst. Environ.* **2023**. [CrossRef]
18. Cruden, D.M.; Varnes, D.J. Landslides: Investigation and Mitigation. Chapter 3—Landslides Types and Processes. *Transp. Res. Board Spec. Rep.* **1996**, *247*, 36–75.
19. Borrelli, L.; Cofone, G.; Coscarelli, R.; Gullà, G. Shallow Landslides Triggered by Consecutive Rainfall Events at Catanzaro Strait (Calabria–Southern Italy). *J. Maps* **2015**, *11*, 730–744. [CrossRef]
20. Borrelli, L.; Conforti, M.; Mercuri, M. LiDAR and UAV System Data to Analyse Recent Morphological Changes of a Small Drainage Basin. *ISPRS Int. J. Geo Inf.* **2019**, *8*, 536. [CrossRef]
21. Aceto, L.; Caloiero, T.; Pasqua, A.A.A.; Petrucci, O. Analysis of Damaging Hydrogeological Events in a Mediterranean Region (Calabria). *J. Hydrol.* **2016**, *541*, 510–522. [CrossRef]
22. Caloiero, T.; Petrucci, O. The Impact of Damaging Hydrogeological Events on Urbanised Sectors: The Case of 19th November 2013 in Catanzaro (Italy). In Proceedings of the 3rd IAHR Europe Congress "Water - Engineering and Research", Porto, Portugal, 14–16 April 2014; pp. 1–8.
23. Petrucci, O.; Pasqua, A.A. Damaging Events along Roads during Bad Weather Periods: A Case Study in Calabria (Italy). *Nat. Hazards Earth Syst. Sci.* **2012**, *12*, 365–378. [CrossRef]
24. Petrucci, O. Brief Communication the Assessment of Damage Caused by Historical Landslide Events. *Nat. Hazards Earth Syst. Sci.* **2013**, *13*, 755–761. [CrossRef]
25. Petrucci, O.; Gulla, G. A Simplified Method for Assessing Landslide Damage Indices. *Nat. Hazards* **2010**, *52*, 539–560. [CrossRef]
26. Petrucci, O.; Gullà, G. A Support Analysis Framework for Mass Movement Damage Assessment: Applications to Case Studies in Calabria (Italy). *Nat. Hazards Earth Syst. Sci.* **2009**, *9*, 315–326. [CrossRef]
27. Brunetti, M.T.; Peruccacci, S.; Rossi, M.; Luciani, S.; Valigi, D.; Guzzetti, F. Rainfall Thresholds for the Possible Occurrence of Landslides in Italy. *Nat. Hazards Earth Syst. Sci.* **2010**, *10*, 447–458. [CrossRef]
28. Peruccacci, S.; Brunetti, M.T.; Gariano, S.L.; Melillo, M.; Rossi, M.; Guzzetti, F. Rainfall Thresholds for Possible Landslide Occurrence in Italy. *Geomorphology* **2017**, *290*, 39–57. [CrossRef]
29. Gariano, S.L.; Petrucci, O.; Guzzetti, F. Changes in the Occurrence of Rainfall-Induced Landslides in Calabria, Southern Italy, in the 20th Century. *Nat. Hazards Earth Syst. Sci.* **2015**, *15*, 2313–2330. [CrossRef]
30. Luca, F.; Robustelli, G.; Conforti, M.; Fabbricatore, D. Geomorphological Map of the Crotone Province (Calabria, South Italy). *J. Maps* **2011**, *7*, 375–390. [CrossRef]
31. Gullà, G.; Conforti, M.; Borrelli, L. A Refinement Analysis of the Shallow Landslides Susceptibility at Regional Scale Supported by GIS-Aided Geo-Database. *Geomat. Nat. Hazards Risk* **2021**, *12*, 2500–2543. [CrossRef]
32. Antronico, L.; Borrelli, L.; Coscarelli, R.; Pasqua, A.A.; Petrucci, O.; Gullà, G. Slope Movements Induced by Rainfalls Damaging an Urban Area: The Catanzaro Case Study (Calabria, Southern Italy). *Landslides* **2013**, *10*, 801–814. [CrossRef]
33. Buttafuoco, G.; Caloiero, T.; Coscarelli, R. Spatial and Temporal Patterns of the Mean Annual Precipitation at Decadal Time Scale in Southern Italy (Calabria Region). *Theor. Appl. Climatol.* **2011**, *105*, 431–444. [CrossRef]
34. Antronico, L.; Sorriso-Valvo, M.; Tansi, C.; Gullà, G. *Carta Litologico–Strutturale e Dei Movimenti in Massa Della Stretta di Catanzaro (Scala 1:50,000)*; LINEA 2—Previsione e Prevenzione di Eventi Franosi a Grande Rischio; Consiglio Nazionale delle Ricerche, Gruppo Nazionale per la Difesa dalle Catastrofi Idrogeologiche: Florence, Italy, 2001.
35. Gullà, G.; Antronico, L.; Iaquinta, P.; Terranova, O. Susceptibility and Triggering Scenarios at a Regional Scale for Shallow Landslides. *Geomorphology* **2008**, *99*, 39–58. [CrossRef]
36. Monaco, C.; Tortorici, L. Active Faulting in the Calabrian Arc and Eastern Sicily. *J. Geodyn.* **2000**, *29*, 407–424. [CrossRef]
37. Brutto, F.; Muto, F.; Loreto, M.F.; De Paola, N.; Tripodi, V.; Critelli, S.; Facchin, L. The Neogene-Quaternary Geodynamic Evolution of the Central Calabrian Arc: A Case Study from the Western Catanzaro Trough Basin. *J. Geodyn.* **2016**, *102*, 95–114. [CrossRef]
38. Maesano, F.E.; Tiberti, M.M.; Basili, R. The Calabrian Arc: Three-Dimensional Modelling of the Subduction Interface. *Sci. Rep.* **2017**, *7*, 8887. [CrossRef]
39. Pirrotta, C.; Barberi, G.; Barreca, G.; Brighenti, F.; Carnemolla, F.; De Guidi, G.; Monaco, C.; Pepe, F.; Scarfì, L. Recent Activity and Kinematics of the Bounding Faults of the Catanzaro Trough (Central Calabria, Italy): New Morphotectonic, Geodetic and Seismological Data. *Geosciences* **2021**, *11*, 405. [CrossRef]
40. Van Dijk, J.P.; Bello, M.; Brancaleoni, G.P.; Cantarella, G.; Costa, V.; Frixa, A.; Golfetto, F.; Merlini, S.; Riva, M.; Torricelli, S. A Regional Structural Model for the Northern Sector of the Calabrian Arc (Southern Italy). *Tectonophysics* **2000**, *324*, 267–320. [CrossRef]
41. Longhitano, S.G.; Chiarella, D.; Muto, F. Three-dimensional to Two-dimensional Cross-strata Transition in the Lower Pleistocene Catanzaro Tidal Strait Transgressive Succession (Southern Italy). *Sedimentology* **2014**, *61*, 2136–2171. [CrossRef]
42. Calcaterra, D.; Parise, M. Weathering in the Crystalline Rocks of Calabria, Italy, and Relationships to Landslides. *Geol. Soc. Lond. Eng. Geol. Spec. Publ.* **2010**, *23*, 105–130. [CrossRef]
43. Borrelli, L.; Perri, F.; Critelli, S.; Gullà, G. Minero-Petrographical Features of Weathering Profiles in Calabria, Southern Italy. *Catena* **2012**, *92*, 196–207. [CrossRef]
44. Cianflone, G.; Dominici, R. Physical Stratigraphy of the Upper Miocene Sedimentary Succession in the Northeastern Catanzaro Through (Central Calabria, Italy). *Rend. Online Soc. Geol. Ital.* **2011**, *17*, 63–69.

45. Pulice, I.; Scarciglia, F.; Leonardi, L.; Robustelli, G.; Conforti, M.; Cuscino, M.; Lupiano, V.; Critelli, S. Studio Multidisciplinare Di Forme e Processi Denudazionali Nell'area Di Vrica (Calabria Orientale). *Mem. Soc. Geogr. Ital.* **2009**, *87*, 403–417.
46. Conforti, M.; Borrelli, L.; Cofone, G.; Gullà, G. Exploring Performance and Robustness of Shallow Landslide Susceptibility Modeling at Regional Scale Using Different Training and Testing Sets. *Environ. Earth Sci.* **2023**, *82*, 161. [CrossRef]
47. Gariano, S.L.; Petrucci, O.; Rianna, G.; Santini, M.; Guzzetti, F. Impacts of Past and Future Land Changes on Landslides in Southern Italy. *Reg. Environ. Chang.* **2017**, *18*, 437–449. [CrossRef]
48. Conforti, M.; Ietto, F. Modeling Shallow Landslide Susceptibility and Assessment of the Relative Importance of Predisposing Factors, through a GIS-Based Statistical Analysis. *Geosciences* **2021**, *11*, 333. [CrossRef]
49. Conforti, M.; Ietto, F. Influence of Tectonics and Morphometric Features on the Landslide Distribution: A Case Study from the Mesima Basin (Calabria, South Italy). *J. Earth Sci.* **2020**, *31*, 393–409. [CrossRef]
50. Petrucci, O.; Versace, P. ASICal: A Database of Landslides and Floods Occurred in Calabria (Italy). In Proceedings of the 1st Italian-Russian Workshop: New Trends in Hydrology, CNR-GNDCI, Rende, Italy, 24–26 September 2002.
51. Polemio, M.; Petrucci, O. The Occurrence of Floods and the Role of Climate Variations from 1880 in Calabria (Southern Italy). *Nat. Hazards Earth Syst. Sci.* **2012**, *12*, 129–142. [CrossRef]
52. Brázdil, R.; Chromá, K.; Dolák, L.; Řehoř, J.; Řezníčková, L.; Zahradníček, P.; Dobrovolný, P. Fatalities Associated with the Severe Weather Conditions in the Czech Republic, 2000–2019. *Nat. Hazards Earth Syst. Sci.* **2021**, *21*, 1355–1382. [CrossRef]
53. Pereira, S.; Zêzere, J.L.; Quaresma, I.; Santos, P.P.; Santos, M. Mortality Patterns of Hydro-Geomorphologic Disasters. *Risk Anal.* **2016**, *36*, 1188–1210. [CrossRef]
54. Papagiannaki, K.; Petrucci, O.; Diakakis, M.; Kotroni, V.; Aceto, L.; Bianchi, C.; Brázdil, R.; Gelabert, M.G.; Inbar, M.; Kahraman, A. Developing a Large-Scale Dataset of Flood Fatalities for Territories in the Euro-Mediterranean Region, FFEM-DB. *Sci. Data* **2022**, *9*, 166. [CrossRef]

Disclaimer/Publisher's Note: The statements, opinions and data contained in all publications are solely those of the individual author(s) and contributor(s) and not of MDPI and/or the editor(s). MDPI and/or the editor(s) disclaim responsibility for any injury to people or property resulting from any ideas, methods, instructions or products referred to in the content.